Results from the NOMAD Experiment

The NOMAD collaboration
presented by
Boris A. Popov* [a]

[a]Laboratory of Nuclear Problems, JINR, 141980 Dubna, USSR

The NOMAD experiment has been searching for $\nu_\mu \leftrightarrow \nu_\tau$ oscillations by looking for the appearance of τ^- in events from the CERN-SPS neutrino beam. With some improvements in the analysis techniques with respect to the previous published results and including data from 1998 run, no evidence for oscillations is found, resulting in an updated limit on the oscillation probability of $P(\nu_\mu \leftrightarrow \nu_\tau) < 0.5 \times 10^{-3}$ at 90% C.L. This corresponds to a limit on the oscillation mixing angle of $\sin^2 2\theta_{\mu\tau} < 1.0 \times 10^{-3}$ for large Δm^2. By using the 1% contamination of ν_e in the neutrino beam we can also exclude $\nu_e \leftrightarrow \nu_\tau$ oscillations and set a limit on the probability of $P(\nu_e \leftrightarrow \nu_\tau) < 3 \times 10^{-2}$ at 90% C.L. ($\sin^2 2\theta_{e\tau} < 6 \times 10^{-2}$ at large Δm^2).

1. Introduction

NOMAD (Neutrino Oscillation MAgnetic Detector, WA-96) is an experiment searching for $\nu_\mu \leftrightarrow \nu_\tau$ oscillations in the CERN-SPS wide band neutrino beam. Neutrino oscillations are possible if the neutrinos have masses and if their flavour and mass eigenstates are different. In the simplified two flavour scenario, the probability of oscillation is given by:

$$P(\nu_\mu \leftrightarrow \nu_\tau) = \sin^2(2\theta)\sin^2(1.27\Delta m^2 L/E), \quad (1)$$

where $\Delta m^2 = \left|m_1^2 - m_2^2\right|$ is the mass squared difference between the two mass eigenstates, θ is the mixing angle between them, L is the distance between the source and the detector in km and E is the energy of the neutrino in GeV.

Given the average energy of the neutrinos at the CERN-SPS beam and the average distance between the target and the detector (see below), the experiment is sensitive to the cosmologically relevant neutrino mass range ($\Delta m^2 > 1\ eV^2$) and to small mixing angles. Potential ν_τ candidates are identified by the kinematical signatures from the decay of a τ^- produced in a charged current (CC) interaction. The detector is sensitive to 82.5% of the decay modes: $\tau^- \rightarrow e^-\overline{\nu}_e\nu_\tau$, $\tau^- \rightarrow h^-(+n\pi^0)\nu_\tau$ and $\tau^- \rightarrow \pi^+\pi^-\pi^- + n\pi^0 (n \geq 0)\nu_\tau$. This talk updates the results already published [1,2], which were based on 1995-1997 data, by more sensitive analyses including the data collected during 1998 run (which was the last year of NOMAD data taking).

2. CERN Neutrino Beam

The CERN West Area neutrino beam [3] uses 450 GeV/c protons from the SPS accelerator. These protons impinge on a beryllium target, 110 cm long, producing secondary mesons (mainly pions and kaons) that are focused with two magnetic focusing elements, the horn and the reflector. These secondary particles are allowed to decay in a 290 m vacuum decay tunnel, with 369 m of iron and earth shielding used as an absorber. The total distance between the beryllium target and NOMAD setup is 835 m, while the average distance between the production point of the neutrino and the detector is only 620 m.

The beam is made up of predominantly ν_μ, but a GEANT [4] simulation of the beamline predicts contaminations of 6.1% of $\overline{\nu}_\mu$, 0.9% of ν_e and 0.2% of $\overline{\nu}_e$ in the neutrino flux. The corresponding neutrino spectra are shown in Figure 1. The intrinsic contamination of ν_τ (from D_s decays) has been calculated to provide a ratio of 5×10^{-6} ν_τ CC interactions with respect to ν_μ CC interactions in NOMAD [5], a negligible background given the sensitivity of the experiment.

*popov@nusun.jinr.dubna.su

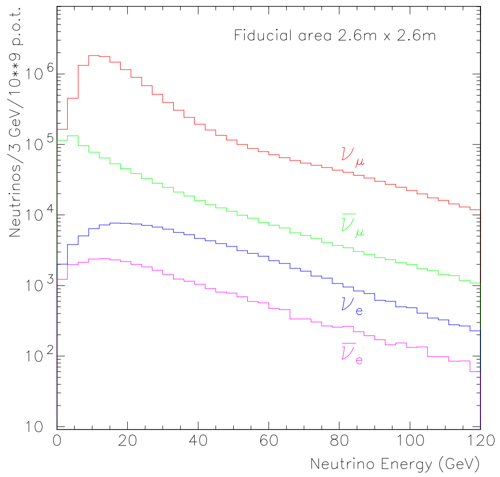

Figure 1. Flux predictions for the different neutrino species within a 2.6 m× 2.6 m fiducial area at the NOMAD detector.

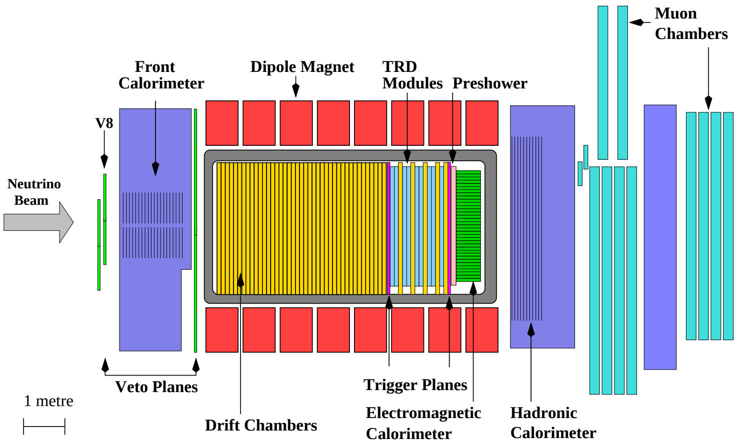

Figure 2. Side view of the NOMAD detector.

3. NOMAD detector

A schematic view of the NOMAD apparatus can be found in Figure 2 and the detector has been described in more detail elsewhere [6]. It consists of an active target of 44 drift chambers, with a total fiducial mass of 2.7 *tons*, within a 0.4 T dipole magnetic field. The drift chambers serve the double role of acting as a target mass and the tracking medium. The average density of the drift chamber volume is 0.1 g/cm^3 with each drift chamber providing only 2% of a radiation length. The momentum resolution is approximately 3.5% for momenta less than 10 GeV/c.

Electron identification is achieved with a transition radiation detector (TRD) [7] made of 9 modules with each module consisting of a polypropylene radiator followed by a plane of straw tubes. The pion rejection achieved is 10^3 with a 90% electron efficiency (for isolated tracks). A lead-glass electromagnetic calorimeter [8] provides an energy resolution of $3.2\%/\sqrt{E(GeV)} \oplus 1\%$ and a preshower detector provides additional electron identification (a pion rejection of 10^2 for an electron efficiency of 90%). A hadronic calorimeter is used for hadron identification and a set of muon chambers provide a muon detection efficiency of 97% for momenta greater than 5 GeV/c.

4. Analysis Strategy

The resolution of the drift chambers is not sufficient to observe the τ candidate directly, as in the case of CHORUS experiment [9] which uses nuclear emulsion. The recognition of potential ν_τ CC interactions is achieved by the identification of the τ decay products using kinematical criteria.

4.1. Kinematical method

There are two main criteria used in NOMAD to separate between ν_τ candidates and background events:

- **Isolation of the τ decay products from the hadronic jet.** In a ν_τ CC interaction in which the τ decays, for example, to a pion, the pion is isolated with respect to the hadronic jet. On the other hand, a pion from a ν_μ neutral current background event is part of the hadronic jet. An isolation variable Q_T, which is the component of the momentum of visible τ decay prod-

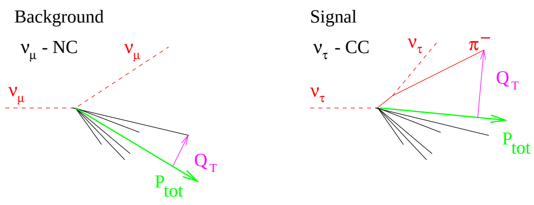

Figure 3. Isolation of the τ decay candidate (a pion in this example) for ν_μ NC and ν_τ CC.

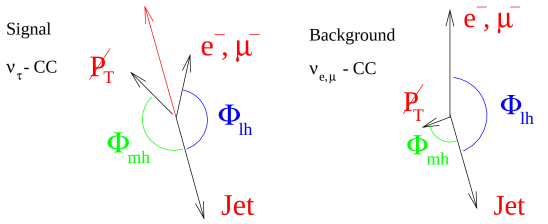

Figure 4. Kinematic configuration in the transverse plane for a ν_τ CC and a background ν_μ or ν_e CC.

ucts perpendicular to the total visible momentum vector, can be used to isolate the decay products (see Figure 3).

- **Kinematical configuration in the plane perpendicular to the incoming neutrino direction**. In the transverse plane one can identify the following vectors (see Figure 4): $p_T^{\vec{l}}$ which is the transverse momentum of the outgoing lepton, $p_T^{\vec{J}et}$ the transverse momentum of the hadronic jet and $\vec{\not p}_T$ the missing transverse momentum. For a ν_τ CC event the missing transverse momentum is due to the undetected neutrinos from the τ decay, while in the case of a ν_e CC background event this quantity is on average smaller and is mainly due to undetected neutrals, reconstruction failures and nucleon Fermi motion. The amount of imbalance is related to the magnitude of the missing momentum and related to the transverse mass variable: $M_T = \sqrt{(|\vec{\not p}_T| + |p_T^{\vec{l}}|)^2 - (p_T^{\vec{J}et})^2}$. The direction of the imbalance is also important, as can be seen in Figure 4 because the angle between the missing transverse momentum and the transverse momentum of the hadronic jet (Φ_{mh}) in the ν_τ CC is generally larger than in the background from ν_μ and ν_e CC interactions. The angle Φ_{lh} between the transverse momenta of the lepton and the hadronic jet will be normally smaller in the signal than in the background.

4.2. Likelihood functions

None of the variables used to perform the separation of τ candidates from background can unambiguously make the τ selection. The strength of NOMAD lies in the combination of these different kinematic variables to perform the separation. NOMAD uses the likelihood technique to make the combinations of the relevant kinematic variables (for example, Φ_{mh}, Φ_{lh}, Q_T, M_T). A likelihood function is the product of the probability distribution functions for each of the variables or set of variables (one can also make multidimensional functions that take into account correlations among the variables). The logarithm of the ratio of likelihood functions for signal and background describes the degree of separation between them.

4.3. Data simulator

The level of background rejection of the order of 10^5 requires the use of techniques that can simulate the behaviour of our data over five orders of magnitude. Due to differences in the simulation and reconstruction mainly of the hadronic system, it is not expected that our Monte Carlo (MC) reproduce the data to this accuracy. For example, the missing p_T distribution is not well reproduced by the data [1,2] so NOMAD has adopted the data simulator technique to overcome this problem.

The data simulator (DS) is based on the assumption that one can calculate the expected background and the efficiency to the signal by using the data. This is achieved by commencing from an identified ν_μ CC event, removing the muon and substituting it by another lepton. If the lepton is a neutrino, this corresponds to a fake NC event, if it is an electron it is a fake ν_e CC event and if it is a τ, followed by its subsequent decay, then a fake ν_τ CC event is simulated. One has to make a further correction to eliminate any charge and energy bias and threshold effects that might ensue. Furthermore, one can apply the identical procedure to Monte Carlo data and produce samples of Monte Carlo simulator (MCS) events.

The comparison of the difference between the DS and MCS samples is a direct measure of the differences between the hadronic system behaviour in the data and in the Monte Carlo simulation. The signal and background efficiencies are then calculated as follows:

$$\epsilon = \epsilon_{MC} \times \frac{\epsilon_{DS}}{\epsilon_{MCS}}, \tag{2}$$

where ϵ_{MC} is the efficiency of the MC, ϵ_{DS} is the efficiency of the DS and ϵ_{MCS} is the efficiency of the MCS.

4.4. Blind analysis

Another feature of the NOMAD analysis is the application of a "blind box" approach. A blind box is defined around the region where we expect the signal to appear and all cuts and corrections are performed outside of the signal region to show that the analysis is robust and can reproduce the data where we don't expect the signal to be strong. A further cross-check can be applied in which the data and MC are compared for an equivalent analysis selecting positive candidates since a τ^+ signal from oscillations is not expected.

The position of the box is selected at the level in which the sensitivity is minimum (or stable). The sensitivity is defined as the average upper limit that would be obtained from an ensemble of experiments with the expected background and no true signal [10]. Additionally, one can create several bins inside the box region that can enhance the global sensitivity of the experiment due to the variation in the ratio of signal to background as a function of bin. An unbiased choice of the closed box region and its internal bins ensures the robustness of the result. Once the analysis is well understood then one is allowed to "open the box" and see if there is an excess of signal above the expected background in the signal region.

5. Search for $\nu_\mu \leftrightarrow \nu_\tau$ Oscillations

5.1. $\tau^- \to e^-\overline{\nu}_e\nu_\tau$ channel

The most sensitive channel available to NOMAD is the electronic decay of the τ, due to the reduced background from the $\sim 1\%$ ν_e background and the excellent electron identification capabilities of the NOMAD detector. The data set used for this analysis corresponds to all available data (from 1995 to 1998 runs) consisting of approximately 1.3×10^6 ν_μ CC events.

The selection of the electron candidate is carried out by imposing that there only be one prompt electron in the event emerging from the primary vertex ($\Delta z < 15\ cm$) and that it is identified as an electron by the TRD, preshower and electromagnetic calorimeter. The energy of the electron has to be above 1.5 GeV and it should not be consistent with a photon conversion (the invariant mass between the electron candidate and any positive track should be greater than 50 MeV).

The rejection of NC interactions is achieved by a multidimensional likelihood function which is a measure of the "isolation" of the electron candidate and includes the following variables: $\theta_{\nu T}$, the angle between the incident neutrino direction and the total momentum of the event; $\theta_{\nu h}$, the angle between the incident neutrino direction and the total hadron momentum; θ_{MIN}, the minimum angle between the electron momentum and any momentum of the hadrons; Q_T; the electron energy and the transverse mass M_T.

The rejection of ν_μ and ν_e CC interactions is achieved with a second likelihood function which measures the momentum imbalance in the transverse plane and which contains the following variables: the transverse momentum of the electron, the transverse momentum of the hadronic jet, Φ_{lh}, the total visible energy of the event, $\theta_{\nu T}$ and Q_{lep}, the electron momentum component perpendicular to the hadronic jet momentum. The dis-

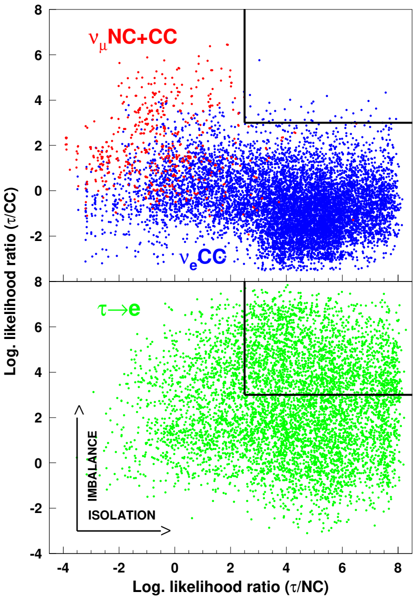

Figure 5. Likelihood ratios for CC rejection and NC rejection for Monte Carlo background and $\tau \rightarrow e$ signal. The signal box is defined in the top right corner.

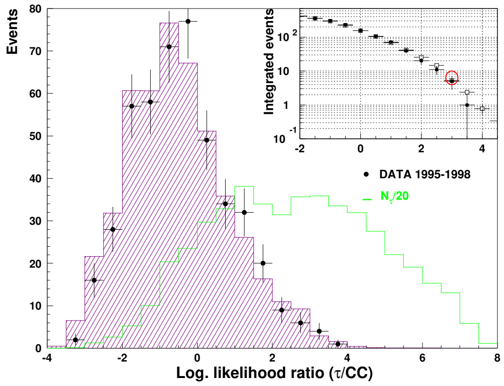

Figure 6. Data simulator corrected log likelihood function to reject CC events for the signal (dotted histogram), for the background (hashed histogram) and for the data (dots). The integral distribution is also shown in the top right corner.

tribution of Monte Carlo background and signal events for a scatter plot of the two likelihood functions are shown in Figure 5. The box in the upper right hand corner defines the signal region and this has been divided into six bins at the later stage of the analysis.

After applying the data simulator corrections to the Monte Carlo predictions one obtains excellent agreement with the data for all the e^+ in the whole likelihood range and for the e^- in the region outside of the signal box. After opening the box, the number of events found is consistent with the expected background (see Figure 6).

The total number of events remaining in the signal region is 5, consistent with a background of 5.3 ± 0.8 distributed in the six bins as shown in Table 1 and Figure 7. If the oscillation probability would have been 1, there would have been 4110 τ^- candidates, so there is no evidence for oscillations in this τ^- decay channel.

5.2. $\tau^- \rightarrow h^- + X$ channel

The analysis of the hadronic one prong decay of the τ has also been performed with the full (1995 to 1998) data sample. The selection of the hadron candidate is achieved by imposing a veto on ν_μ CC and ν_e CC events. All events with a primary muon or electron are rejected. In addition, events with a high p_T track ($p_T > 0.8\ GeV/c$) outside the acceptance of the lepton identification detectors (eg. muon chambers and electromagnetic calorimeter) are also rejected, to avoid CC events in which the lepton escapes identification. The hadron decay candidate is selected as the track with the highest or second highest p_T track in the event.

The rejection of NC and CC background is achieved by forming a three dimensional likelihood function with the following variables: Q_T, the transverse mass M_T and

Table 1
Results of the analysis in the $\tau^- \to e^-$ channel.

Bin	N_τ	Exp. Background	Data
1	178	$1.15^{+0.26}_{-0.17}$	2
2	208	$0.53^{+0.23}_{-0.12}$	1
3	903	$0.28^{+0.31}_{-0.09}$	0
4	654	2.13 ± 0.23	2
5	473	0.98 ± 0.16	0
6	1694	0.25 ± 0.09	0
Total	4110	5.3 ± 0.8	5

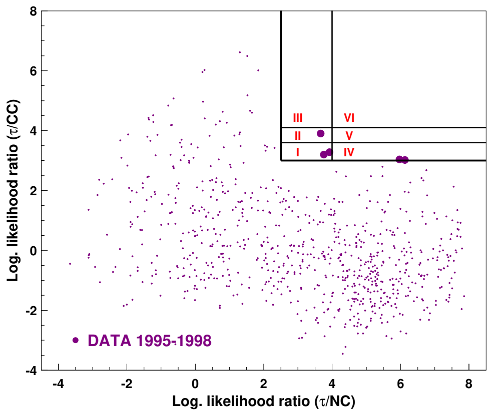

Figure 7. Distribution of the data events in the plane formed by the two likelihood functions. The upper right corner is the signal region divided into six bins with the surviving candidates.

$\rho_m = \frac{|\not{p}_T|}{|\vec{p}_T^{\,h}|+|\vec{p}_T^{\,Jet}|+|\not{p}_T|}$. The isolation of the hadron candidate is achieved by Q_T and the separation of the NC and the signal populations is obtained by the transverse plane variables (M_T and ρ_m) as is shown in Figure 8.

A further two variables, the ratio of the hadron candidate momentum to the visible energy and the transverse momentum of the hadronic jet, complete the description of the global likelihood. Figure 9 contains the likelihood ratio for the τ signals and the NC and CC background. Two bins above a likelihood of 7.2 make up the signal

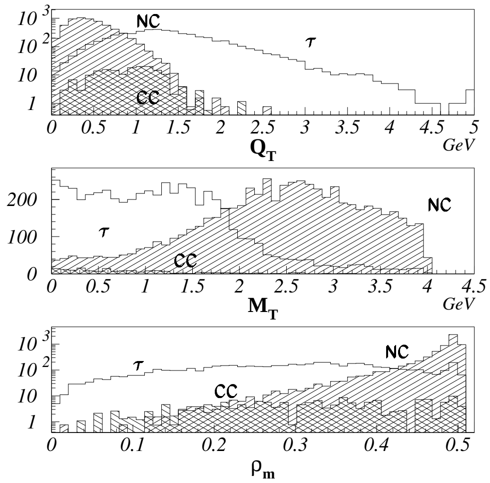

Figure 8. Variables used for the $\tau^- \to h^- + X$ likelihood functions.

Table 2
Results of the analysis in the $\tau^- \to h^-$ channel.

Likelihood	N_τ	Exp. Background	Data
7.2-9.0	918	4.4 ± 1.9	3
> 9.0	1133	2.4 ± 0.8	3
Total	2232	6.8 ± 2.1	6

box. The total number of observed events inside this region is 6, consistent with an estimated background of 6.8 ± 2.1 (see Table 2).

5.3. Other τ^- decay channels

Other channels used in the analysis are the exclusive $\tau^- \to \rho^- \nu_\tau$ in which the ρ^- decays into a $\pi^-\pi^0$ and the $\tau^- \to \pi^+\pi^-\pi^-\nu_\tau$. Both of these analyses use the kinematical constraints associated with the intermediate resonance (the a_1^- in the case of the 3π case). All the previous analyses have been carried out for the case in which the ν_τ undergoes a deep inelastic interaction (DIS) and the data analysed encompass the runs from 1995 to 1998 (1995 to 1996 in the case of the 3π channel). In addition, we have low multiplic-

Table 3
Summary of $\nu_\mu \leftrightarrow \nu_\tau$ search for the various channels.

Channel	Data	Exp. Background	N_{obs}	N_τ
$\tau \to e^- \nu_\tau \overline{\nu}_e$ DIS	95-98	5.3 ± 0.8	5	4110
$\tau \to e^- \nu_\tau \overline{\nu}_e$ LM	95	$0.5^{+0.6}_{-0.2}$	0	218
$\tau^- \to h^-(+n\pi^0)\nu_\tau$ DIS	95-98	6.8 ± 2.1	6	2232
$\tau^- \to h^-(+n\pi^0)\nu_\tau$ LM	95	$0.1^{+0.3}_{-0.1}$	1	198
$\tau \to \rho^- \nu_\tau$ DIS	95-98	$7.3^{+2.2}_{-1.2}$	9	2547
$\tau^- \to \pi^-\ \pi^-\ \pi^+ \nu_\tau$ DIS	95-96	6.5 ± 1.1	5	1180
$\tau^- \to \pi^-\ \pi^-\ \pi^+(+n\pi^0)\nu_\tau$ LM	95	$0.4^{+0.6}_{-0.4}$	0	108

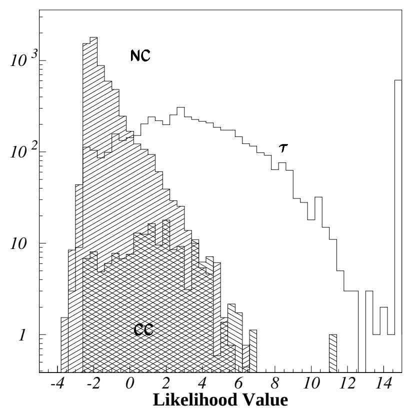

Figure 9. Log likelihood ratio for the $\tau^- \to h^-$ analysis.

ity (LM) analyses which are rich in quasi-elastic and resonance events, but these have not been updated since our published result [1] using only 1995 data. The updated summary with all the channels studied up to now is included in Table 3.

6. Results and Conclusion

From Table 3, the background estimates are in good agreement with the number of events found in the data once the blind boxes are open. There is no evidence for an oscillation signal so NOMAD can set a new limit on the oscillation probability based on the unified approach which is now recommended by the Particle Data Group [10]: $P(\nu_\mu \to \nu_\tau) < 0.5 \times 10^{-3}$ at 90% C.L., improved with respect to our previously published result [2]. This limit is comparable to that obtained by CHORUS [9]. A 90% confidence limit exclusion plot in the $\Delta m^2 - \sin^2 2\theta$ plane can be derived and this is shown in Figure 10. At large Δm^2 the limit on the mixing angle is $\sin^2 2\theta_{\mu\tau} < 1.0 \times 10^{-3}$.

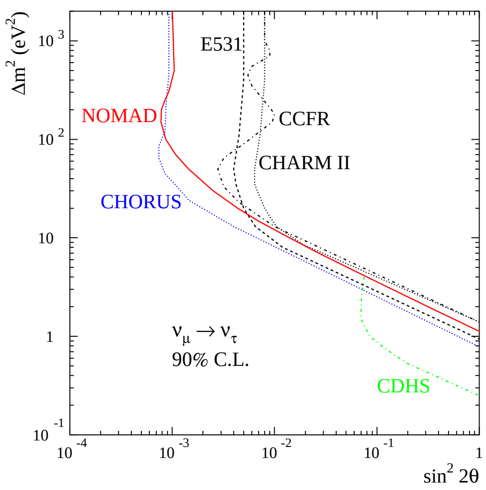

Figure 10. NOMAD 90% C.L. exclusion plot for $\nu_\mu \leftrightarrow \nu_\tau$ oscillations.

In addition, due to the $\sim$ 1% contamination of ν_e in the beam one can also set a $\nu_e \leftrightarrow \nu_\tau$

oscillation probability limit of $P(\nu_e \leftrightarrow \nu_\tau) < 3 \times 10^{-2}$ at 90% C.L. and its associated exclusion plot is shown in Figure 11. The resulting mixing angle would be $\sin^2 2\theta_{e\tau} < 6 \times 10^{-2}$ at large Δm^2.

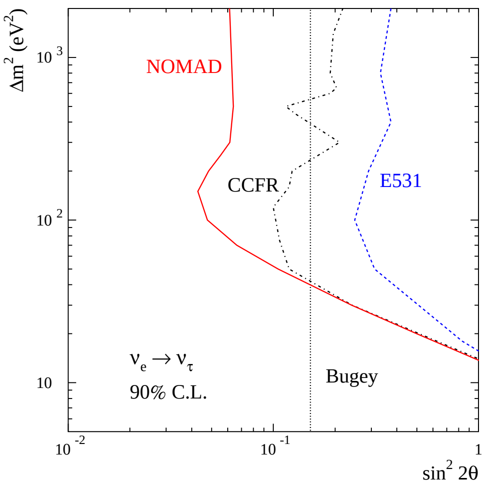

Figure 11. NOMAD 90% C.L. exclusion plot for $\nu_e \leftrightarrow \nu_\tau$ oscillations.

NOMAD has set limits for $\nu_\mu \leftrightarrow \nu_\tau$ oscillations based on all data analysed (about 1.3×10^6 ν_μ CC interactions from 1995 to 1998 runs for some of the τ decay channels). 1998 run was the last year of NOMAD data taking. The quality of the event reconstruction and the analysis efficiencies are still being improved. Addition of the channels that have not been updated for the 1996, 1997 and 1998 data, will hopefully provide further improvement in the sensitivity of the NOMAD analysis in the future.

REFERENCES

1. NOMAD Collaboration, J. Altegoer *et al.*, Phys. Lett. B 431 (1998) 219.
2. NOMAD Collaboration, P. Astier *et al.*, Phys. Lett. B 453 (1999) 169.
3. G. Acquistapace *et al.*, CERN-ECP 95-14 (July 1995).
4. GEANT, CERN Programming Library Long Writeup W5013.
5. B. Van de Vyver, Nucl. Instr. and Meth. A 385 (1997) 91; M.C. González-García and J.J. Gómez-Cadenas, Phys. Rev. D 55 (1997) 1297.
6. NOMAD Collaboration, J. Altegoer *et al.*, Nucl. Instr. and Meth. A 404 (1998) 96.
7. G. Bassompierre *et al.*, Nucl. Instr. and Meth. A 403 (1998) 363; G. Bassompierre *et al.*, Nucl. Instr. and Meth. A 411 (1998) 63.
8. D. Autiero *et al.*, Nucl. Instr. and Meth. A 373 (1996), 358; D. Autiero *et al.*, Nucl. Instr. and Meth. A 387 (1997), 352; D. Autiero *et al.*, Nucl. Instr. and Meth. A 411 (1998), 285.
9. CHORUS Collaboration, E. Eskut *et al.* Nucl. Instr. and Meth. A 401 (1997) 7; CHORUS Collaboration, E. Eskut *et al.* Phys. Lett. B 424 (1998) 202; M. Messina, CHORUS Collaboration, XXXIVth Rencontres de Moriond "Electroweak Interactions and Unified Theories", Les Arcs, March 13-20 1999.
10. G.J. Feldman and R.D. Cousins, Phys. Rev. D 57 (1998) 3873; Particle Data Group, C. Caso *et al.*, Eur. Phys. J. C 3, 172-177.